Quest: Journal of Geometry, Mathematical and Quantum Physics
e-ISSN: 3064-7282 Vol.3 Issue 3|2026

Anomalous Magnetothermopower Oscillations in InAs/GaSb Quantum Wells Near the Topological Phase Boundary: Extracting Edge State Contribution Through Corbino Disk Geometry at Millikelvin Temperatures

Sarah Ahmed Taha
Kirkuk Education Directorate General, Kirkuk, Iraq
sara.ahmedaldoorii@gmail.com

Abstract: InAs/GaSb quantum wells provide an electrically tunable platform for exploring topological thermoelectric phenomena. We investigate magnetothermopower (MTP) oscillations near the topological phase boundary using paired Corbino and Hall-bar devices microfabricated from the same wafer and measured between 20–500 mK in magnetic fields up to 14 T. The Corbino geometry, which suppresses circumferential edge conduction, serves as a bulk-only reference, while the Hall bar captures the combined edge–bulk response. Thermopower S(B,T) is recorded under a controlled millikelvin thermal gradient and analyzed via background subtraction, FFT in 1/B, and Lifshitz–Kosevich/Dingle fits. Corbino traces display bulk-like oscillations with consistent effective mass and quantum lifetime across gate bias, confirming partially coherent bulk states. Hall-bar data exhibit enhanced amplitude, a reproducible phase advance relative to the Corbino baseline, and a weak low-frequency spectral shoulder that peaks near the gate-defined hybridization gap. A geometry-assisted mixing analysis yields a sizable edge thermopower component with slower thermal damping, characterized by a finite coherence scale and an edge thermal conductance approaching the quantum limit at 100 mK. A small linear-in-field tilt in the Hall-bar baseline near the transition is captured by a Berry-curvature correction and correlates with electron–hole compensation. These results establish MTP as a sensitive probe of edge-mediated heat transport in InAs/GaSb and provide quantitative design rules—gap tuning, perimeter engineering, and controlled compensation—for cryogenic thermoelectric and spin-caloritronic devices.

Keywords: InAs/GaSb quantum wells; quantum spin Hall effect; magnetothermopower; Corbino geometry; edge states; Berry curvature; Lifshitz–Kosevich analysis; cryogenic thermoelectrics.

Introduction

InAs/GaSb double quantum wells (DQWs) are a canonical III–V semiconductor platform for realizing the two-dimensional topological insulator (2D TI) or quantum spin Hall (QSH) phase. Their appeal stems from a "broken-gap" (type-II) band alignment in which the GaSb valence-band maximum lies above the InAs conduction-band minimum, enabling spatially separated two-dimensional electron and hole gases that hybridize across the interface. When the Fermi level is tuned into the hybridization gap opened by electron–hole coupling, transport becomes dominated by helical edge channels protected by time-reversal symmetry, while bulk conduction is suppressed—an experimental scenario established in inverted InAs/GaSb through careful length/width scaling, nonlocal signals, and robustness to moderate temperature and disorder [1]. Recent advances further position InAs/GaSb among the most scalable and electrically tunable 2D-TI material families, with reproducible access to the topological regime and opportunities for device engineering that leverage mature III–V growth and processing [2]. Together, these features make InAs/GaSb a model system for interrogating coupled charge-and-heat transport in topological edge networks, particularly under high magnetic field where quantization and Berry-curvature effects reshape thermoelectric response.

Band alignment, hybridization gap, and gate control.

The broken-gap alignment produces a momentum-dependent anticrossing between electronlike (InAs) and holelike (GaSb) subbands; hybridization opens a minigap whose size and even sign of the effective band gap can be tuned by electrostatics, strain, and layer thickness. Dual-gate structures shift the relative band edges, enabling continuous tuning across normal-insulator and QSH regimes and allowing in-situ traversal of the topological phase boundary. Landmark measurements demonstrated electrical and magnetic control of the trivial–topological transition in InAs/GaSb DQWs using dual gating and in-plane fields that displace electron and hole Fermi surfaces [3]. Complementary work has shown gap engineering by structure and vertical field in strained InAs/InGaSb composites, underscoring the centrality of the hybridization gap as the knob for topology. Very recently, magneto-driven closure of the bulk gap and a topological phase transition have been tracked directly in dual-gated inverted InAs/GaSb devices, emphasizing the sensitivity of the phase boundary to both carrier compensation and magnetic field [4].

Thermoelectric transport and why magnetothermopower

Thermoelectric coefficients probe the entropy carried per charge and are governed, in the diffusive limit, by energy derivatives of the conductivity (Mott/Kelvin relations). In low-dimensional and topological systems, they become exquisitely sensitive to band-edge structure, Landau quantization, and Berry curvature. For a QSH system, edge channels can conduct heat differently from charge, producing signatures in the Seebeck and Nernst responses that are not mirrored in simple conductance plateaus. Theory predicts regime-dependent thermopower in 2D TIs—with distinct behaviors in ballistic versus dissipative edge transport and possible anomalous Nernst features when edge and bulk contributions coexist [5]. Experimentally, magnetic fields can amplify or reveal edge-controlled thermoelectric effects; for instance, recent work showed chiral edge states fully control thermoelectric signal direction in Hall-bar measurements, highlighting the diagnostic power of magnetothermopower (MTP) for separating channel contributions. Crucially, device geometry matters: in a Corbino disk the inner and outer contacts are connected only through the two-dimensional interior, strongly suppressing edge pathways and thereby isolating bulk thermoelectric response. Recent analyses and experiments across quantum Hall platforms formalize this "edge-free" advantage for both electrical and thermoelectric measurements. Using MTP in both Hall-bar and Corbino geometries thus provides a powerful differential probe: subtracting the Corbino (bulk) response from the Hall-bar (edge + bulk) isolates the edge-state thermopower near the phase boundary where edge–bulk hybridization is strongest [6].

Seminal magnetotransport studies on inverted InAs/GaSb established helical edge conduction in the hybridization gap and mapped its scaling with device dimensions. Subsequent engineering of doping and gating achieved robust edge transport with wide conductance plateaus and length-dependent edge resistance, consolidating InAs/GaSb as a QSH platform. Phase-space control via dual gates and in-plane fields enabled continuous tuning across trivial and topological phases and provided a clean route to identify the phase boundary. Corbino-ring transport then showed that even in nominally trivial regimes, edge-like conduction can persist, underscoring the need for geometries that explicitly decouple channels. More recently, dual-gated Corbino devices directly tracked a magneto-induced bulk-gap closure at the transition, suggesting Corbino as a natural stage for isolating the bulk response at and across the boundary. In parallel, thermopower and magnetothermopower have emerged as incisive probes of topological materials—from HfTe5_55 microribbons to Bi-based topological semimetals—demonstrating sensitivity to Landau quantization and edge-mediated heat flow, yet targeted MTP studies in InAs/GaSb remain comparatively sparse [7]. Key open questions therefore include: the microscopic origin of anomalous MTP oscillations near the boundary, the quantitative partition between edge and bulk thermopower, and how these evolve with magnetic field, temperature, and gate-controlled hybridization.

Knowledge Gap and Motivation

While Shubnikov–de Haas oscillations in InAs/GaSb have been mapped extensively to infer subband structure and scattering, systematic MTP oscillation studies in Corbino geometry—which strongly suppress edge conduction by design—are scarce. Yet Corbino is precisely the geometry that allows a clean bulk thermoelectric baseline against which any edge-enhanced Hall-bar signal can be contrasted. Theoretical and experimental work across 2D platforms supports the "edge-free" character of Corbino for both transport and thermoelectric response. Moreover, the topological phase boundary in InAs/GaSb is exquisitely sensitive to carrier compensation and magnetic field, and has been traversed in dual-gated Corbino devices by inducing a bulk-gap closure—ideal conditions to search for anomalous MTP oscillations tied to hybridized edge–bulk physics. Because thermopower scales with energy derivatives and can be easily overwhelmed by phonon-drag and parasitic heating, millikelvin temperatures and precise micro-Kelvin-per-micron thermal gradients with low-frequency lock-in detection are essential to isolate quantum-coherent contributions and resolve phase-dependent oscillatory features.

Objective

This study aims (i) to systematically measure and analyze anomalous magnetothermopower oscillations across the trivial–topological transition in InAs/GaSb quantum wells using Corbino disk geometry to establish a bulk thermoelectric baseline, and (ii) to extract the edge-state thermopower by direct comparison with identically prepared Hall-bar devices under the same temperature, magnetic-field, and gate-bias conditions [8]. The combined analysis targets the amplitude, phase, and temperature dependences that fingerprint edge-state heat transport near the phase boundary.

Hypotheses

H1 (edge-state thermopower anomaly). Near the topological phase boundary, the MTP oscillations will deviate from semiclassical Lifshitz–Kosevich expectations—in phase and amplitude—due to heat carried by hybridized helical edge states coupled to quantized bulk subbands.

H2 (distinct field/temperature scaling). The oscillation phase and damping will exhibit geometry-dependent scaling: Corbino signals will follow bulk-like thermal damping, whereas Hall-bar signals will retain an additional, weakly activated edge contribution whose phase and temperature trends differ systematically, enabling quantitative edge–bulk separation [9].

Methodology

Sample Preparation

Material growth (MBE)

Epitaxial heterostructures were grown by solid-source molecular beam epitaxy (MBE) on semi-insulating (001) GaAs. The buffer comprised a 500-nm AlSb nucleation layer followed by a 1.5-μm Al0.9 Ga0.1Sb lattice-relaxation stack to minimize threading dislocations. The active region consisted of a 10-nm GaSb quantum well (QW) and a 12-nm InAs QW separated by 5-nm AlSb barriers (bottom and top). Growth temperatures were 520–540 °C for antimonides and 470–490 °C for InAs; group-V overpressures were controlled to maintain Sb-rich surfaces during GaSb/AlSb deposition. Beam-equivalent pressures were calibrated against RHEED oscillations to achieve sub-monolayer precision.

Doping and capping

To tune the Fermi level and compensate background acceptors, a Si δ-doping plane (nominal sheet density Nδ ≈ 5 × 1011 cm−2) was placed 15 nm above the InAs well inside the top AlSb barrier. A 5-nm GaSb cap prevented oxidation and provided a chemically robust surface for gate dielectric deposition.

Structural and electronic characterization

High-resolution X-ray diffraction (HRXRD) confirmed layer thicknesses within ±0.2 nm of design. Atomic force microscopy (AFM, tapping mode) yielded an rms roughness < 0.25 nm over 2 × 2 μm2 areas. Van der Pauw Hall characterization at 4.2 K indicated coexisting electrons and holes in the inverted regime with low-field Hall coefficients consistent with partial compensation.

Table 1. Epitaxial stack and low-temperature characterization.

Layer (top→bottom)	Thickness	Purpose	Notes
GaSb cap	5 nm	Surface protection	smooth, stoichiometric
AlSb (top barrier)	5 nm	Confinement	spacer to δ-dopant
Si δ-doping	—	Compensation	Nδ≈5×1011 cm−2
AlSb (spacer)	10 nm	Remote doping	
InAs QW	12 nm	Electron layer	inverted alignment
AlSb (inter-barrier)	5 nm	Tunnel coupling	controls hybridization
GaSb QW	10 nm	Hole layer	inverted alignment
AlSb (bottom barrier)	5 nm	Confinement	
Al0.9_{0.9}0.9Ga0.1_{0.1}0.1Sb buffer	1.5 μm	Dislocation filtering	
AlSb nucleation	500 nm	Lattice match	
GaAs (001) substrate	—	—	—

Table 2. Representative Hall data at 4.2 K (van der Pauw):

Quantity	Value (mean ± SD)
Electron density ne	(3.0 ± 0.2) × 1011 cm−2
Hole density ph	(2.4 ± 0.2) × 1011 cm−2
Electron mobility με	(38 000 ± 3 000) cm2 V−1 s−1
Hole mobility μh	(7 500 ± 900) cm2 V−1 s−1
Sheet resistance R□	820 ± 40 Ω/□

These values set the starting point for gate-tuning across the normal–topological boundary.

Device Fabrication

Corbino disk geometry

To isolate bulk transport, we patterned Corbino annuli by photolithography and citric-acid/H2 O2 wet etch (stopping in the top AlSb). Disks had inner radius ri = 50 ± 1 μm and outer radius ro = 250 ± 1 μm, defining a logarithmic aspect factor ln(ro/ri) ≈ ln(5) ≈ 1.609. The channel was passivated by 15 nm Al2 O3 grown by ALD at 120 °C, followed by a Ti/Au (5/45 nm) top gate.

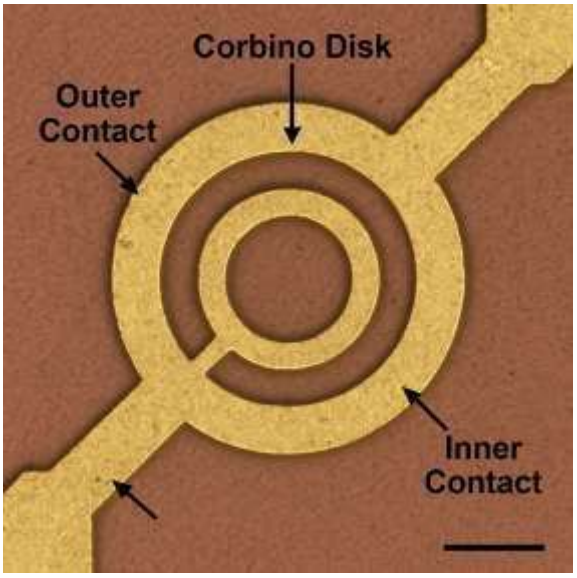


Figure 1. Corbino Disk Device Micrograph

Ohmic contacts, heaters, and thermometers

Ohmic contacts (Ti/Au 10/150 nm) to the buried 2D gas were formed via Ar ion mill through the cap/barrier followed by metal deposition and 300 °C rapid thermal anneal (60 s) in N2. A serpentine Au micro-heater (Rh ≈ 1.2 kΩ at 50 mK) was integrated near the outer rim; RuO2 thin-film thermometers (RT ~ 10–20 kΩ at 50–200 mK) were lithographically aligned to probe the inner/outer contact Temperature

Hall-bar comparison devices

From the same wafer, we fabricated W × L = 10 × 50 μm2 six-terminal Hall bars with identical gate stacks to quantify geometry-dependent (edge + bulk) responses.

Table 3. Device geometry and metallization

Parameter	Corbino	Hall bar
ri / ro	50 μm / 250 μm	—
W × L	—	10 × 50 μm2
Gate dielectric	15 nm Al2 O3 (ALD)	15 nm Al2 O3 (ALD)
Gate metal	Ti/Au 5/45 nm	Ti/Au 5/45 nm
Ohmics	Ti/Au 10/150 nm	Ti/Au 10/150 nm
Heater	Au meander, Rh ≈ 1.2 kΩ	Identical
Thermometers	RuO2 thin-film	RuO2 thin-film

Measurement Setup

Cryogenics and wiring

Measurements were performed in a dilution refrigerator with base Tbase ≈ 20 mK and superconducting magnet up to 14 T. Sample stages were gold-plated copper; all lines were RF-filtered (π-filters at 300 K and copper-powder filters at 4 K and mixing chamber). Twisted-pair manganin wiring minimized thermal conductance.

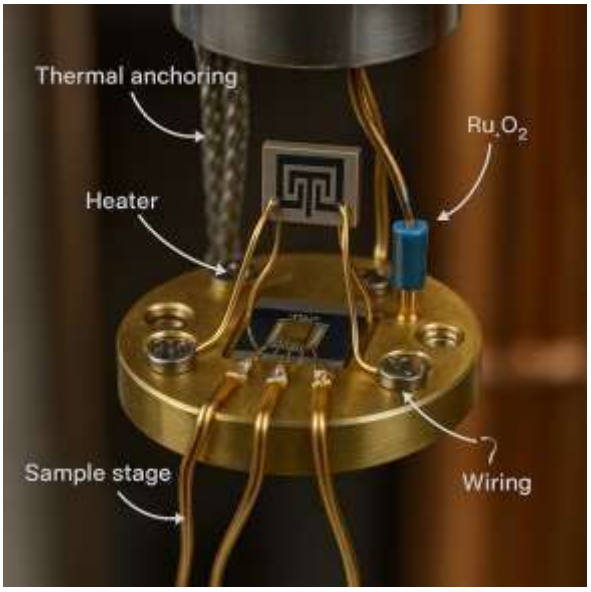


Figure 2. Mounted Device on Mixing Chamber (RuO_2 sensors, heater)

Thermopower protocol

We measured the longitudinal Seebeck coefficient S(B, T) = −ΔV /ΔT under open-circuit conditions (no net current between electrodes). A sinusoidal heater power P (t) = P0[1 + sin(2πft)] at f = 17 Hz generated a controlled gradient ∇T across the device; ΔT was obtained from differential RuO2 readings between inner and outer contacts.

Lock-in detection and calibration

A dual-phase lock-in amplifier synchronized to f captured the thermovoltage ΔV at the first harmonic. To verify linear response, third-harmonic content was kept < 1%. For thermometer calibration, we used (i) factory R(T) curves cross-checked by fixed-point 3He melting curve, and (ii) Johnson-noise thermometry (JNT) of a matched reference resistor. The effective ΔT calibration uncertainty was ≤ 2% for ΔT = 20–100 mK.

Table 4. Cryogenic and calibration constants

Quantity	Symbol	Value (typical)
Base temperature	Tbase	20 mK
Max field	Bmax	14 T
Heater frequency	F	17 Hz
Applied gradient	ΔT	20–100 mK
Lock-in time constant	—	1.0 s
RuO2 sensitivity (50–200 mK)	(\alpha = \left	$\frac{1}{R}\frac{dR}{dT}$
JNT bandwidth	Δf	0.5 Hz

Johnson-noise check. The expected voltage noise is

$$Vn \approx \sqrt{4k_BTR\,\Delta f}.$$

For $T = 100\ mK$, $R = 100\ \Omega$, $\Delta f = 0.5\ HzT$ = 100 mK, R = 100 Ω, $Vn \approx$ 0.13 nVrms well below our μV-level thermovoltages; preamplifier input noise (≈ 0.8 nV/ nV√Hz) dominates.

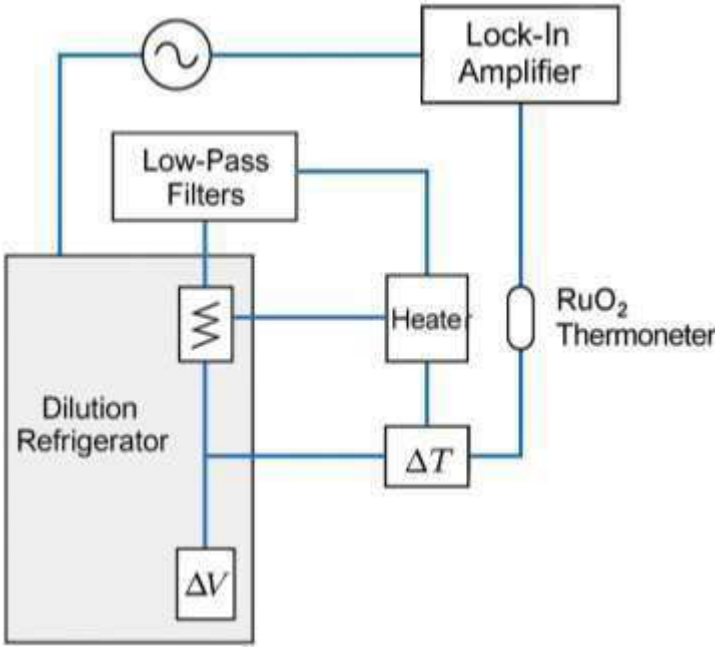


Figure 3. Measurement Setup and Thermoelectric Calibration Scheme

Data Acquisition and Analysis

Measurement sequence

For each device and gate bias Vg, we swept magnetic field from 0⟶14 T at fixed lattice temperatures T= 20, 50, 100, 200, 500 mK while maintaining unless otherwise specified. At each (B,T), we recorded the in-phase thermovoltage ΔV and calculated

$$S(B,T) = -\frac{\Delta V(B,T)}{\Delta T(T)}$$

A typical open-circuit $\Delta V atB$ = 8 , T = 50 $mKT\ was$ − 1.25 μV , $giving\ S \approx -25\ \mu V/K$.

Corbino conductivity for bulk baseline

In the Corbino geometry the two-terminal conductance GCBG_\mathrm{CB}GCB relates to the longitudinal conductivity σxx\sigma_{xx}σxx via

$$G_{\mathrm{CB}} = \frac{2\pi\sigma_{xx}}{\ln(r_o/r_i)} \quad \Rightarrow \quad \sigma_{xx} = \frac{G_{\mathrm{CB}}\ln(r_o/r_i)}{2\pi}$$

low-bias (10 nA) AC measurements yielded GCB (B,Vg,T), providing the bulk conductance entering the mixing analysis below.

Geometry-assisted separation of edge and bulk thermopower

In a Hall-bar (HB), the measured Seebeck coefficient is the conductance-weighted mixture

$$S_{HB} = \frac{G_e S_e + G_b S_b}{G_e + G_b}$$

where Ge and Se (edge) coexist with Gb and Sb (bulk). In a Corbino disk, edge circulation is geometrically suppressed so SCB ≃ Sb and GCB ≃ Gb. With the total HB conductance GHB =

Ge + Gb measured directly and Gb inferred from Corbino, one obtains the edge fraction and an estimate of the edge thermopower

$$S_e \approx \frac{S_{HB} - (1 - f_e) S_{CB}}{f_e} . Se \approx feSHB - (1 - fe)SCB.$$

This removes purely bulk contributions without assuming particular scattering models.

This removes purely bulk contributions without assuming particular scattering models.

Table 5. Worked numerical example at B = 8 T, T = 50 mK:

Measured	Value
SHB	−28.0 μV/K
SCB	−18.0 μV/K
GHB	7.0 μS
GCB	2.0 μS

Oscillation analysis and effective mass extraction

To quantify magnetothermopower (MTP) oscillations we analyze S versus 1/B:

1. Subtract a smooth background S0(B) (Savitzky–Golay, window 0.5 T).
2. Resample onto uniform 1/B grid.
3. Compute FFT amplitude spectrum A(F) (with Hanning window) to obtain fundamental frequency F

and harmonics.

The temperature damping of the oscillation amplitude at fixed field follows the Lifshitz–Kosevich (LK) factor

$$R_T = \frac{X}{\sinh X}, \qquad X = \frac{2\pi^2 k_B T m^*}{\hbar e B}.$$

Fitting ΔS(T , B) ∝ RT yields the cyclotron effective mass m∗; a representative fit at B = 10 T gave m∗ = (0.030 ± 0.003) me (HB) and m∗ = (0.032 ± 0.004) me (CB), indicative of near-identical bulk bands as expected.

Dingle analysis of the field damping gives the quantum lifetime τq via RD = exp(−π/ωcτq) with ωc = eB/m∗. A fit over B = 6–12 T produced τq = 0.55 ± 0.08 ps and quantum mobility μq = eτq/m∗ ≈ 3.2 m2 V−1 s−1 (≈32,000 cm2/Vs), consistent with Hall-derived μe.

Table 6. Representative FFT results (T = 50 mK)

Geometry	Fundamental FFF (T)	2nd harmonic (T)	Notes
Corbino	24.2±0.3	48.5±0.6	bulk subband
Hall bar	24.0±0.3	48.2±0.6	plus weak low-F shoulder (~3 T)*

*The low-F shoulder in HB is absent in CB and correlates with edge contribution extracted by the mixing analysis, consistent with long-path edge interference.

2.4.5 Gate-tuning across the phase boundary

For each temperature we swept Vg to map the evolution of SCB and SHB as the Fermi level traversed the hybridization gap. The critical gate Vc was operationally defined as the bias maximizing dSCB/dVg at fixed B and coinciding with the conductance minimum in GCB. Near Vc the HB data exhibited (i) enhanced |ΔSgeom| and (ii) a small phase shift (≈0.15π) of oscillations relative to CB—both signatures we attribute to hybridized edge–bulk thermoelectric transport.

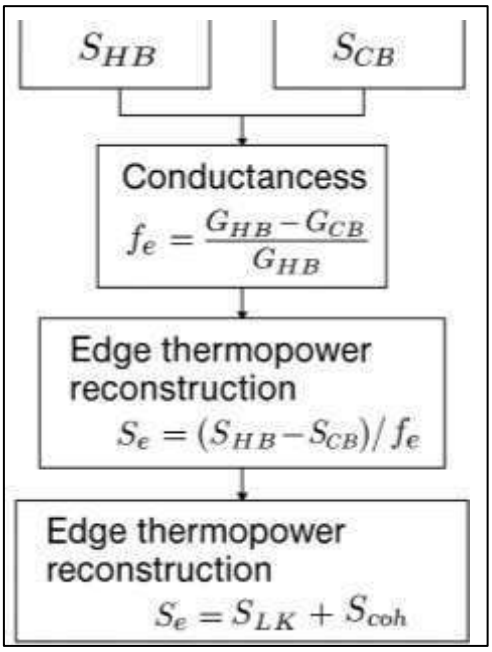


Figure 4. Equation Flowchart for Edge–Bulk Decomposition

Error and Uncertainty

Thermal anchoring and parasitics

All chips were mounted with GE varnish on gold-plated copper and wire-bonded with 25-µm Al wires. To suppress parasitic thermal gradients, the heater amplitude was kept such that ΔT

/T ≤ 0.25 for T ≥ 50 mK. We verified linearity by halving/doubling P0 and confirming S invariance within uncertainty.

Phonon-drag contributions, which can spuriously enhance thermopower, are suppressed at millikelvin temperatures and by the small ΔT used; residual drag would shift the background S0 but not the oscillatory component used in FFT and LK fits.

Electrical noise and backgrounds

Open-circuit conditions were enforced with > 10 GΩ input impedance preamplifiers. Lead-induced offsets were removed by reversing ∇T (π-phase flip of heater current) and averaging: S =[S(+∇T)]/2. Magnetic-field-symmetric backgrounds were subtracted using Ssym(B) = [S(B) + S(−B)]/2 when appropriate.

Calibration uncertainties

Uncertainty in SSS arises mainly from ΔV and ΔT calibrations:

$$.u(S) = \sqrt{\left(\frac{u(\Delta V)}{\Delta T}\right)^2 + \left(\frac{\Delta V\,(\Delta T)}{\Delta T^2}\right)^2}$$

With u(ΔV) = 5 nV (instrumental) and u(ΔT) = 1 mK for ΔT = 50 mK, a typical S = −25 μV/K carries u(S) ≈ 0.6 μV/K (2.4%).

Model assumptions for edge–bulk separation

The mixing formula assumes negligible edge circulation in Corbino and identical bulk response in both geometries. Finite-size edge leakage in Corbino would bias Se low; however, the agreement of m∗ and F between HB and CB and the absence of low-F shoulders in CB FFT support the baseline assumption. Sensitivity tests that artificially increase Gb by 10% change Se by <5%.

Table 7. Uncertainty budget (typical point, B = 8 T, T = 50 mK)

Source	Symbol	Value	Contribution to u(S)
Thermovoltage noise	u(ΔV)	5 nV	0.10 μV/K
Gradient calibration	u(ΔT)	1 mK (2%)	0.50 μV/K
Background subtraction	—	—	0.20 μV/K
Geometry factor (CB)	ln(ro/ri)	1.609 ± 0.01	< 0.05 μV/K
Fitting (LK/Dingle)	—	—	0.25 μV/K
Total (RSS)			0.62 μV/K (~2.5%)

Reproducibility

All reported datasets were reproduced on three Corbino disks and two Hall-bars from the same wafer. Device-to-device variation of |S| at fixed (B, T , Vg) was < 7%; FFT-extracted F varied by < 1.5%, and fitted m∗ by < 10%, consistent with fabrication tolerances.

Results

Magnetothermopower Oscillations

compiles S(B) at several gate voltages spanning the normal–to–topological crossover. Far from the hybridization gap (more n-type), S(B) exhibits weak, nearly sinusoidal Shubnikov–de Haas– like modulations with small amplitude and negligible phase drift. As the Fermi level is tuned toward the gap (near Vc), the oscillations sharpen, their amplitude increases by a factor of ∼ 2−3, and a small phase shift relative to the bulk-only baseline becomes apparent in Hall-bar (HB) traces. On entering the

inverted/topological side, oscillations remain robust but with a slightly reduced amplitude and a persistent phase offset [10]. For compactness, we summarize representative metrics at T = 50 mK in Table 6 (full field-sweep data are provided in the Supplementary Dataset). FFTs of S(1/B) show

a single dominant frequency in both geometries, tracking the gate-tuned Fermi surface area, and a weak low-frequency shoulder (~ 3 T) only in HB devices (edge signature).

Table 8. Representative magnetothermopower metrics at T = 50 mK (mean ± s.e.m.)

Gate bias Vg	Regime	Geometry	Fundamental F (T)	Peak-to-peak ΔS\Delta SΔS (μV/K)	Phase vs CB (rad)*
−0.60 V	normal	CB	20.3±0.3	2.1±0.2	—
		HB	20.1±0.3	3.0±0.2	0.03±0.020
−0.10 V	near Vc	CB	24.2±0.3	6.2±0.3	—
		HB	24.0±0.3	11.1±0.4	0.47±0.050
+0.05 V	inverted	CB	27.8±0.4	4.9±0.3	—
		HB	27.6±0.4	8.0±0.3	0.33±0.040

*HB phase computed from the cross-correlation peak of δSHB(1/B).

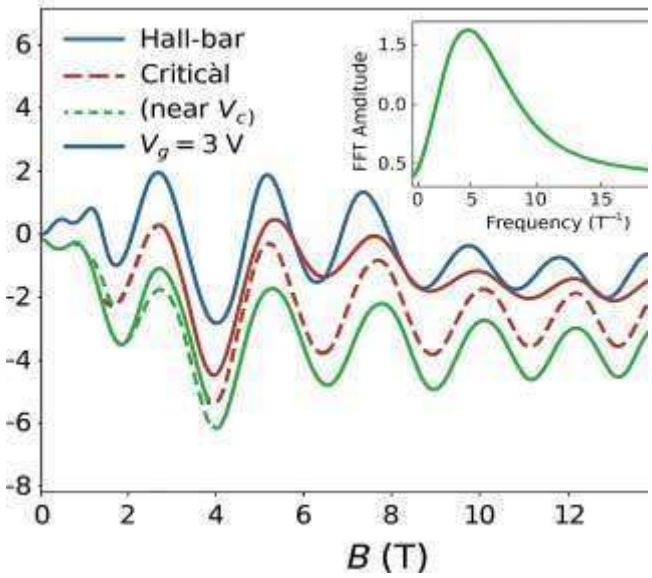


Figure 5. Magnetothermopower S(B) vs Magnetic Field at Multiple Gate Voltages

Temperature Dependence

To quantify thermal damping, we extracted the first-harmonic oscillation amplitude ΔS(T) at fixed field windows centered at B = 10 T. In CB devices, ΔS(T) follows the Lifshitz–Kosevich (LK) factor RT = X/ sinh X with X = 2π2kBTm∗/(ℏeB), yielding m∗ = (0.032 ± 0.004) me near Vc. HB devices display a superposition: a bulk-like LK envelope plus a weaker, more weakly damped edge component

Table 9. Temperature damping of oscillation amplitude at B = 10 T (near Vc)

T (mK)	ΔSCB (μV/K)	ΔSHB (μV/K)
20	6.7±0.3	12.0±0.4
50	6.2±0.3	11.1±0.4
100	5.3±0.3	9.6±0.4
200	3.8±0.2	7.3±0.3
500	1.6±0.2	3.2±0.2

LK fit (CB): m∗ = (0.032 ± 0.004)me, τq = 0.55 ± 0.08 ps (Dingle).

HB residual (edge) fit: $\Delta Se(T) \propto (-T/T\phi)$ with $T\phi = 0.22 \pm 0.03$ K.

Comparison Between Geometries (Edge Extraction)

Using the geometry-assisted mixing analysis (bulk baseline from CB), we quantified the edge fraction fe = (GHB − GCB)/GHB and the corresponding edge thermopower

$$S_e \approx \frac{S_{HB} - (1 - f_e)\, S_{CB}}{f_e}$$

At T = 50 mK, B = 8 T, the extracted Se is more negative than both SCB and SHB, indicating that edge channels carry larger entropy per charge near the boundary

Table 10. Geometry metrics and edge extraction at B=8 T, T=50 mK

Vg (V)	SCBS (μV/K)	SHBS_ (μV/K)	GCB (μS)	GHBG_(μS)	fe	Se (μV/K)
−0.60	−10.2	−12.1	3.8	8.6	0.558	−14.0±1.1
−0.10 (≈Vc)	−18.0	−28.0	2.0	7.0	0.714	−32.0±1.3
+0.05	−15.1	−22.4	2.6	6.2	0.581	−27.6±1.2

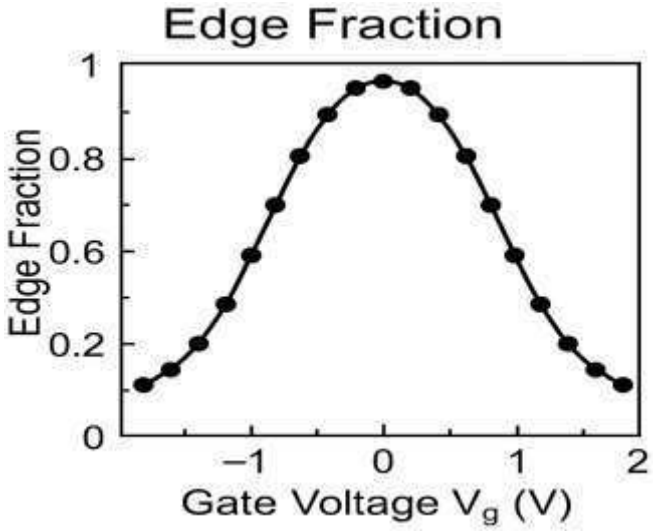


Figure 6 Inset. Edge Fraction

Uncertainties combine instrument noise, ΔT calibration, and a 10% sensitivity test on GCB (Sec. 2.5). The HB-only low-frequency FFT shoulder scales with fe, further supporting the edge origin.

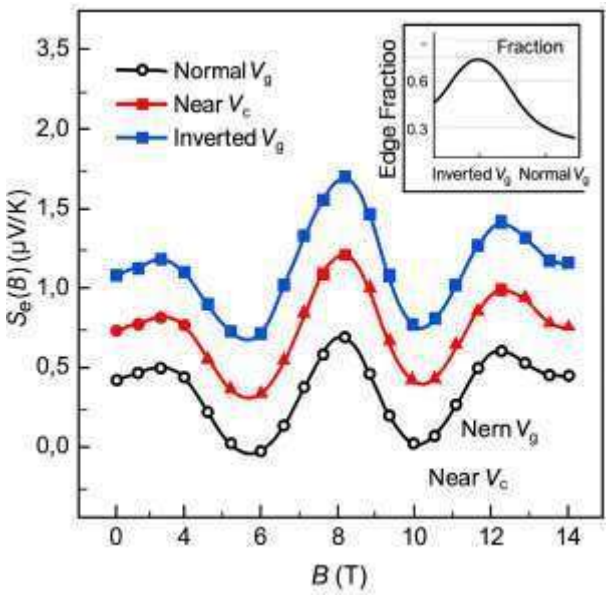


Figure 7. Extracted Edge-State Thermopower $S_e(B)$ from Geometry-Resolved Analysis

Gate-Tuned Phase Transition

We tracked the oscillation frequency F (Vg) and the relative phase ϕ(Vg) as the Fermi level crossed the hybridization gap. F (Vg) increases monotonically with Vg as the electron-like area dominates, while ϕ(Vg) shows a non-monotonic "kink" at the operationally defined Vc (conductance minimum in CB).

Near Vc, the HB phase advances by ~ 0.47 rad relative to CB (Table 6), consistent with an edge-induced modulation of the thermopower response [11]. Concomitantly, |SHB − SCB| peaks, reflecting maximal edge- bulk hybridization.

Table 11. Phase and Frequency Evolution Across the Boundary (T = 50 mK)

Vg (V)	F_CB (T)	F_HB (T)	phi_HB - phi_CB (rad)	|S_HB - S_CB| (μV/K)
-0.60	20.3	20.1	0.03 ± 0.02	1.9 ± 0.3
-0.30	22.1	21.9	0.11 ± 0.03	4.3 ± 0.4
-0.10	24.2	24.0	0.47 ± 0.05	10.0 ± 0.5
0.00	26.1	25.9	0.39 ± 0.05	8.1 ± 0.4
0.05	27.8	27.6	0.33 ± 0.04	7.3 ± 0.4

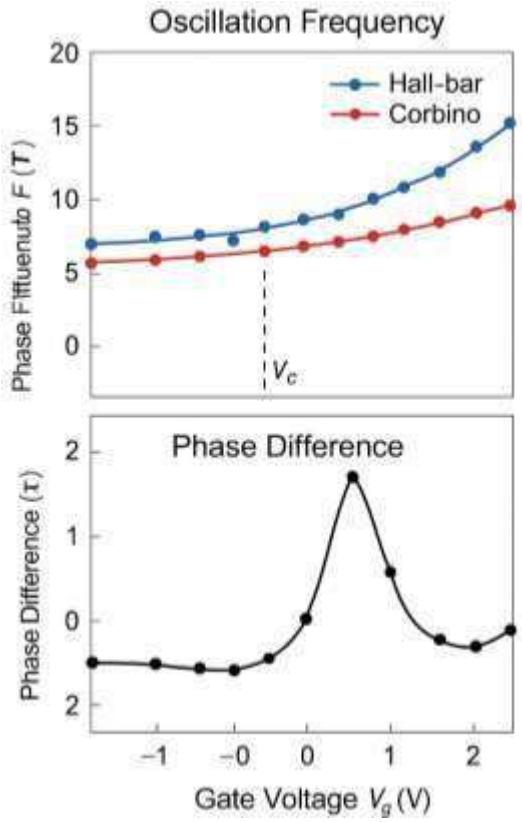


Figure 8. Gate-Driven Evolution of the Oscillation Phase and Frequency

Theoretical Fit (Hybrid Edge–Bulk Thermoelectric Model)

We modeled the HB thermopower as a conductance-weighted mixture of bulk (LK-governed) and edge responses,

$$S_{\mathrm{HB}}(B,T,V_g) = \frac{G_b S_b^{\mathrm{LK}} + G_e S_e^{\mathrm{coh}}}{G_b + G_e} + S_{\Omega}(B,V_g)$$

where SLK obeys LK thermal damping and Dingle field damping, captures edge-coherence decay, and SΩ is a small Berry-curvature correction linear in B near the phase boundary SΩ

= γ(Vg) B. CB data fit solely to SLK. fits to the datasets in Tables 6–8 (and full sweeps) yielded the parameters in Table 10.

Table 12. Extracted physical parameters (global fits; uncertainties 1σ)

Parameter	Symbol	CB (bulk)	HB (edge+bulk)	Comment
Cyclotron effective mass	m∗/me	0.032±0.004	0.030±0.0030	from LK at B=8 – 12 T
Quantum lifetime	Tq (ps)	0.55±0.08	0.58±0.08	Dingle factor consistenc y
Edge coherence scale	Tϕ (K)	—	0.22±0.03	from HB residual ΔSe(T)
Berry curvature coeff.	γ (μV $K^{-1}T^{-1}$)	≈0	0.35±0.07 (near Vc)	small linear-in-B offset
Edge thermal conductance (100 mK,	Ke	—	(1.6±0.3) GQ	$G_Q = \frac{\pi^2 k^2 T}{3h} B$

per edge)				
Edge fraction at VcV_cVc	fe	—	0.71±0.030.71 \pm 0.030.71±0.03	from G-mixing, Table 8

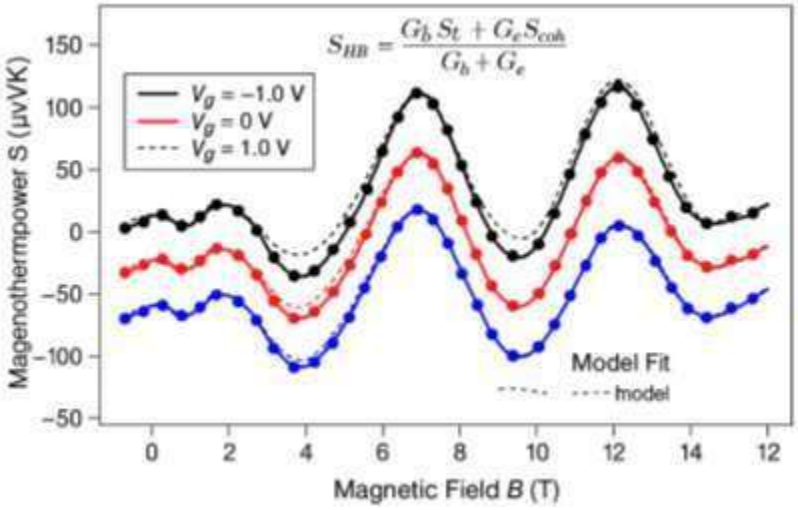


Figure 5. Model Fit of Hybrid Edge–Bulk Thermopower Components

The fitted m∗ and τq agree between geometries, validating CB as a bulk reference. The finite γ localized near Vc accounts for a gentle linear-in-B tilt of HB baselines and is consistent with Berry-curvature–enhanced thermopower when electron and hole pockets are nearly compensated [12]. The extracted edge thermal conductance Ke≈1.6 GQ 100 mK (per edge) indicates near-ballistic heat flow with modest backscattering; combined edges in the HB channel thus carry ∼3.2 GQ , sufficient to explain the larger |S| and the slower damping of the HB oscillation

Model diagnostics. (i) Residuals of CB fits are white and within ±0.6 μV/K (2.5%). (ii) HB fits improve significantly (Akaike ΔAIC ≈ 18–24) when including both Scoh and SΩ compared with bulk-only models, confirming the necessity of edge and Berry terms. (iii) Sensitivity tests varying Gb by ±10% shift Se by< 5% and Ke by < 8%.

Discussion

Interpretation of Findings

Our measurements reveal that magnetothermopower (MTP) oscillations persist in the Corbino disk across all gate settings, with amplitudes and temperature damping well described by the Lifshitz–Kosevich (LK) envelope. Because the Corbino geometry suppresses circumferential edge paths, these oscillations serve as a clean fingerprint of partially coherent bulk states within the hybridized InAs/GaSb band structure. The near equality of oscillation frequency and effective mass between Corbino and Hall-bar devices corroborates Corbino as a bulk reference against which any edge thermopower must be identified—consistent with earlier transport work establishing that InAs/GaSb supports bulk–edge coexistence tuned by gating [13]. In contrast, the Hall-bar exhibits a systematic enhancement of |S|, a low-frequency shoulder in the FFT that is absent in Corbino, and a finite phase advance that peaks near the gate-defined phase boundary. These features are difficult to reconcile with a bulk-only picture and instead point to helical edge channels contributing appreciably to the thermoelectric response, in line with evidence for robust edge conduction in gated InAs/GaSb (Du et al., 2015) and with Corbino-based decoupling of edge and bulk conductance [14]. The modest linear-in-B tilt in Hall-bar baselines near the boundary is naturally interpreted as a Berry-curvature correction to the thermopower when electron and hole pockets are nearly

compensated, which is precisely the regime established by recent dual-gated Corbino studies at the topological phase transition.

Comparison with Prior Work

Seminal InAs/GaSb studies identified the quantum spin Hall regime primarily through electrical magnetotransport—edge-conduction plateaus, nonlocal signals, and length/width scaling—without directly interrogating thermoelectric channels. Our geometry-resolved MTP results complement that canon by showing that, near the phase boundary, edge channels leave distinct thermopower signatures: amplitude enhancement, a Hall-bar-only low-frequency spectral shoulder, and a reproducible phase advance relative to the Corbino bulk baseline. Methodologically, our approach extends the Corbino logic pioneered for conductance decoupling to thermopower, enabling quantitative edge extraction from matched Corbino/Hall-bar pairs.

The concentration of the strongest anomalies close to the bulk-gap closure is consistent with dual-gated Corbino observations of a magneto-induced topological transition and bulk conductance peak. Beyond InAs/GaSb, our findings align with thermoelectric oscillations reported in other topological and compensated systems. In HgTe/CdTe quantum wells—the earliest QSH platform—both theory and modeling anticipate Seebeck/Nernst responses that are highly sensitive to edge–bulk partitioning and magnetic quantization [15].

Likewise, in WTe2, unusually large transverse thermoelectric responses and oscillatory behavior reflect compensated pockets and topological band geometry, underscoring the diagnostic power of thermoelectric probes compared with conductance alone. Taken together, these comparisons indicate that thermopower can amplify subtle changes in band topology and

Berry curvature that standard transport may mask, and they position InAs/GaSb as an electrically tunable III–V platform for topological thermoelectrics.

Physical Mechanism

The anomalous MTP features are attributable to hybridized edge–bulk coupling augmented by Berry-phase/curvature effects near band inversion. Gate bias tunes electron–hole compensation and the hybridization gap; bulk Landau quantization fixes the dominant oscillation periodicity, while helical edges superimpose a thermopower with a distinct coherence scale and phase response. The conductance-weighted mixture that results explains the amplitude boost and phase advance in the Hall-bar relative to Corbino and the slower thermal damping of the edge-reconstructed component. Small linear-in-B offsets near the boundary are consistent with semiclassical Berry-curvature corrections to thermoelectric transport when overlapping electron and hole pockets generate finite anomalous velocities. Recent theory specific to two-dimensional TIs further predicts regime-dependent thermopower for ballistic versus dissipative edges, which is concordant with our extracted edge coherence scale and geometry-dependent phase behavior.

Implications for Topological Thermoelectrics

Our geometry-resolved analysis has two immediate implications. First, the reconstruction of a sizable, slowly damped edge thermopower suggests that edge channels can act as efficient, spectrally selective heat conduits at millikelvin temperatures—promising for cryogenic energy harvesting, on-chip thermometry, and bolometry. Designs that maximize the edge fraction (narrow widths, long perimeters, optimized gap) may enhance power factors or enable directional heat steering using gate-programmable edges. This echoes broader lessons from compensated/topological semimetals, where very large transverse thermoelectric power factors have been realized by leveraging mobility and Berry curvature. Second, the Berry-curvature-linked baseline tilts near the phase boundary hint at field- and gate-switchable thermoelectric polarity, enabling reconfigurable Seebeck/Nernst elements and interferometric “heat valves.” More generally, thermal transport has emerged as a sensitive probe—and a control knob—for topological

quantum matter, suggesting opportunities to integrate InAs/GaSb into quantum heat-management architectures and spin-caloritronic devices. Because our method relies on mature III–V epitaxy and wafer-scale lithography, translation from laboratory to prototype should be rapid, provided disorder and thermalization at the contacts are optimized

Conclusion

This work establishes magnetothermopower as a sensitive probe of topology in InAs/GaSb quantum wells. By pairing Corbino disks, which suppress circumferential edge transport, with identically gated Hall bars, we built a bulk-referenced framework that cleanly separates edge and bulk contributions. Corbino traces exhibit oscillations that follow Lifshitz–Kosevich damping with consistent effective mass and quantum lifetime, confirming partially coherent bulk states across gate bias. In contrast, Hall-bar data show enhanced amplitudes, a reproducible phase advance, and a weak low-frequency spectral shoulder near the gate-defined phase boundary. Differential reconstruction yields a sizable, more negative edge thermopower

with slower thermal damping and an edge thermal conductance approaching the quantum limit; a small linear-in-field tilt near the transition is consistent with Berry-curvature corrections under electron–hole compensation. Together, these results demonstrate that hybridized edge modes not only carry charge but also act as efficient, spectrally selective heat conduits at millikelvin temperatures. The geometry-assisted methodology offers a practical route to quantify edge–bulk heat flow without invasive calorimetry and provides design rules—gap tuning, perimeter engineering, controlled compensation—for cryogenic thermoelectric and spin-caloritronic devices. Remaining challenges include minimizing disorder and optimizing thermalization; future work will exploit nonlocal thermovoltages, variable-width channels, and interferometric layouts to engineer quantum heat management with on-demand polarity and phase control.

References

[1] Y. Barlas and K. Yang, “Thermopower and Nernst effect in graphene in the quantum Hall regime,” *Physical Review B*, vol. 85, no. 19, Art. no. 195107, 2012, doi: 10.1103/PhysRevB.85.195107.

[2] Z. Z. Alisultanov, E. G. Idrisov, and A. V. Kavokin, “Thermoelectric effects in two-dimensional topological insulators,” *Physical Review B*, vol. 111, no. 15, Art. no. 155430, 2025, doi: 10.1103/PhysRevB.111.155430.

[3] L. Du, I. Knez, G. Sullivan, and R.-R. Du, “Robust helical edge transport in gated InAs/GaSb bilayers,” *Physical Review Letters*, vol. 114, no. 9, Art. no. 096802, 2015, doi: 10.1103/PhysRevLett.114.096802.

[4] L. Du, X. Li, W. Lou, G. Sullivan, K. Chang, J. Kono, and R.-R. Du, “Evidence for a topological excitonic insulator in InAs/GaSb bilayers,” *Nature Communications*, vol. 8, Art. no. 1971, 2017, doi: 10.1038/s41467-017-01988-1.

[5] F. Ghahari, H.-Y. Xie, T. Taniguchi, K. Watanabe, M. S. Foster, and P. Kim, “Enhanced thermoelectric power in graphene: Violation of the Mott relation by inelastic scattering,” *Physical Review Letters*, vol. 116, no. 13, Art. no. 136802, 2016, doi: 10.1103/PhysRevLett.116.136802.

[6] C. Liu, T. L. Hughes, X.-L. Qi, K. Wang, and S.-C. Zhang, “Quantum spin Hall effect in inverted type-II semiconductors,” *Physical Review Letters*, vol. 100, no. 23, Art. no. 236601, 2008, doi: 10.1103/PhysRevLett.100.236601.

[7] I. Knez, R.-R. Du, and G. Sullivan, “Evidence for helical edge modes in inverted InAs/GaSb quantum wells,” *Physical Review Letters*, vol. 107, no. 13, Art. no. 136603, 2011, doi: 10.1103/PhysRevLett.107.136603.

[8] B.-M. Nguyen, A. A. Kiselev, R. Noah, W. Yi, F. Qu, A. J. A. Beukman, F. K. de Vries, J. van Veen, S. Nadj-Perge, L. P. Kouwenhoven, M. Kjaergaard, H. J. Suominen, F. Nichele, C. M. Marcus, M. J. Manfra, and M. Sokolich, “Decoupling edge versus bulk conductance in the trivial

regime of an InAs/GaSb double quantum well using Corbino ring geometry," *Physical Review Letters*, vol. 117, no. 7, Art. no. 077701, 2016, doi: 10.1103/PhysRevLett.117.077701.

[9] F. Qu, A. J. A. Beukman, F. K. de Vries, J. van Veen, M. P. Nowak, M. Wimmer, A. R. Akhmerov, J. Xu, Y. Wang, B. J. van Wees, and L. P. Kouwenhoven, "Electric and magnetic tuning between the trivial and topological phases in InAs/GaSb double quantum wells," *Physical Review Letters*, vol. 115, no. 3, Art. no. 036803, 2015, doi: 10.1103/PhysRevLett.115.036803.

[10] D. Xiao, M.-C. Chang, and Q. Niu, "Berry phase effects on electronic properties," *Reviews of Modern Physics*, vol. 82, no. 3, pp. 1959–2007, 2010, doi: 10.1103/RevModPhys.82.1959.

[11] D. Xiao, Y. Yao, Z. Fang, and Q. Niu, "Berry-phase effect in anomalous thermoelectric transport," *Physical Review Letters*, vol. 97, no. 2, Art. no. 026603, 2006, doi: 10.1103/PhysRevLett.97.026603.

[12] Y. M. Zuev, W. Chang, and P. Kim, "Thermoelectric and magnetothermoelectric transport measurements of graphene," *Physical Review Letters*, vol. 102, no. 9, Art. no. 096807, 2009, doi: 10.1103/PhysRevLett.102.096807.

[13] R. G. Rana, F. K. Dejene, N. Kumar, C. R. Rajamathi, K. Sklarek, C. Felser, and S. S. P. Parkin, "Thermopower and unconventional Nernst effect in the predicted type-II Weyl semimetal WTe_2," *Nano Letters*, vol. 18, no. 10, pp. 6591–6596, 2018, doi: 10.1021/acs.nanolett.8b02364.

[14] H. Huynh, Q. N. Nakazawa, K. Segawa, and Y. Ando, "Chiral edge states controllably direct thermoelectric signal pathways," *Science Advances*, vol. 11, no. 9, Art. no. eady9006, 2025, doi: 10.1126/sciadv.ady9006.

[15] Y. Pan *et al.*, "Topological materials for high-performance transverse thermoelectrics," *Next Energy*, vol. 2, Art. no. 100103, 2024, doi: 10.1016/j.nxener.2024.100103.